Failure Tolerance through Active Braking: A Kinematic Approach

James D. English

MÄK Technologies
185 Alewife Brook Parkway
Cambridge, MA 02138
jde@mak.com

Anthony A. Maciejewski

Purdue University
1285 Electrical Engineering Building
West Lafayette, IN 47907-1285
maciejew@ecn.purdue.edu

Abstract

For a manipulator operating in a hazardous or remote environment, an important concern is its capability after a component failure, since retrieval or repair is not always possible. Methods have been presented in the literature for optimizing capabilities after specific types of failures. However, techniques for achieving failure tolerance when conversion between failure types is possible has not been fully explored. This paper presents an approach to improving postfailure performance by converting between locked-joint failures and free-swinging failures through active braking. When a manipulator is moved slowly, gravitational forces can be used to control the failed joint in free-swinging mode, allowing the problem to be cast as a kinematic one. The validity of the kinematic formulation and its implementation and global consequences are explored.

KEY WORDS—failure tolerance, free-swinging failure, passive joint, active braking, underactuated manipulator

1. Introduction

Failure tolerance for robotic manipulators has been widely addressed, often with a focus on using kinematic redundancy. A type of failure often addressed is one resulting in a joint locking. Methods for designing a manipulator with a desired postfailure workspace or a desired level of dexterity after a locking failure have been presented (Maciejewski 1991; Paredis, Au, and Khosla 1994; Paredis and Khosla 1994), as have general methods for preparing kinematically redundant manipulators for the possibility of a failure (Lewis and Maciejewski 1994, 1997; Roberts 1996). Similar issues have been addressed for free-swinging failures (those for which actuator torque is lost). Methods of preparing for a free-swinging failure were presented in English and Maciejewski (1998, 2000a), and a study of postfailure capabilities related to design was presented in English and Maciejewski (1997). These techniques will be combined to maximize the postfailure capability of a manipulator by choosing between locked and free-swinging modes of operation and using gravity to control the free-swinging joint when the brakes are released. The two failure modes are illustrated in Figure 1.

Considerable work has been done to address the related issue of controlling a manipulator with free-swinging joints using dynamic coupling, both with brakes and without. In Oriolo and Nakamura (1991), conditions of integrability (i.e., reduction to a holonomic constraint) for free-swinging joints were investigated and methods of stabilizing manipulators without brakes on equilibrium manifolds were presented. In Arai and Tachi (1991a) and Arai, Tanie, and Tachi (1993), active-braking methods were presented based on dynamic coupling. Operational space methods were developed in Arai, Tanie, and Tachi (1993). Optimal choices of braking sequences for multiple free-swinging joints were given in Bergerman and Xu (1998), and robust methods were presented in Bergerman and Xu (1996). These works focus on dynamically controlling passive joints about equilibrium points, not on finding the equilibrium points, and not on exploiting gravitational forces.

This paper addresses a complementary issue: that of controlling passive joints using gravity alone. Methods are presented for converting, through repeatedly activating and releasing individual joint brakes, between locked-joint failures and free-swinging failures for manipulators under gravitational forces. Manipulators used in hazardous and remote environments—those where failure tolerance is likely to be

This work was supported by a NASA graduate student research fellowship (Grant No. NGT9-2) and by Sandia National Laboratories under Contract No. AL-3011.
The International Journal of Robotics Research
Vol. 20, No. 4, April 2001, pp. 287-299,

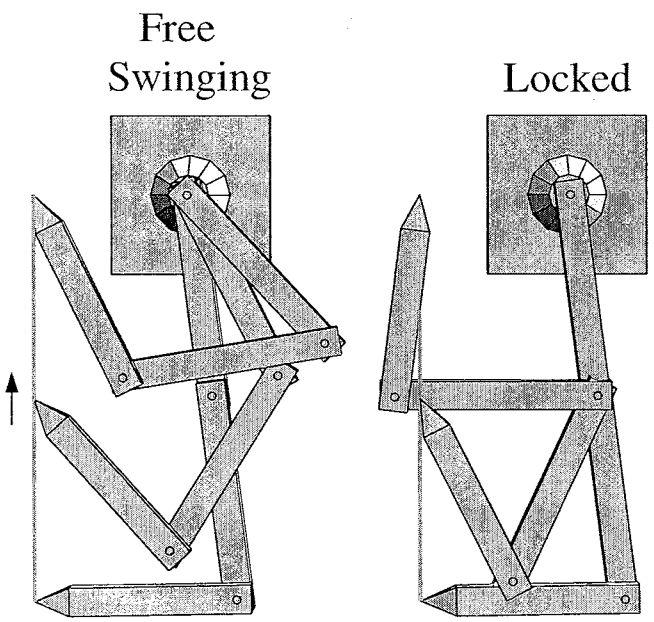

Fig. 1. A three-link planar positioning manipulator is shown tracing a line with joint one free-swinging (left) and locked (right). In the free-swinging case, the arm traces the line while maintaining the composite center of mass of the arm directly below joint one, while in the locked case, the arm traces the line without moving joint one.

an issue—are usually slow moving, and this slow-moving assumption allows the gravitational force–based control problem to be cast as a kinematic one.

The organization of this paper is as follows. Section 2 presents the swing angle, a key kinematic parameter, and provides justifying hardware experiments. Section 3 provides velocity control methods for both free-swinging and locked-joint failure modes. Section 4 examines ways to best switch between failure modes by activating and releasing the joint brakes. Section 5 addresses global aspects of postfailure operation, such as the resulting workspace. Section 6 illustrates the methods through several examples.

2. Swing Angle

An n-DoF manipulator's joint variables are given by

$$\mathbf{q} = [q_1\ q_2\ \cdots\ q_n]^T. \tag{1}$$

A fundamental kinematic parameter for the developments in this paper is the swing angle. The swing angle $\hat{\theta}_i$ is defined as the angle through which rotational joint i would move to settle into a stationary configuration if its actuator torque were removed (English and Maciejewski 1998). This paper will focus on free-swinging failures dominated by viscous friction. Of the common types of robotic drives and mechanisms (Morecki and Knapczyk 1999), this could be the case for catastrophic gear, chain, or belt failure in a transmission mechanism or catastrophic failure in a pneumatic or hydraulic system. For dry-friction-dominated failures, such as those involving low-viscous-friction electric motors, the joint can be freed using an active clutch. For a viscous-friction model, the swing angle equals the smallest-magnitude angular difference between the actual value of joint i and, with the other joints fixed, a value that gives the lowest potential energy (with the value set to π when the smallest magnitude angular difference is $\pm\pi$). The viscous-friction model swing angle will be used here.

2.1. Value and Gradient Calculations

To establish the swing angle, let M_i be the composite mass of links i through n calculated independently of joint type as follows:

$$M_i = m_i + M_{i+1};\ M_n = m_n. \tag{2}$$

Here, m_i is the mass of link i. Using these values, the composite first-moment-of-inertia vector $\vec{s}_i^{\,*}$ as expressed in the ith D-H frame (based on the labeling scheme of Paul 1981) can be calculated using

$$\vec{s}_i^{\,*} = {}^i\mathbf{R}_{i+1}(\vec{s}_{i+1}^{\,*} + \vec{s}_{i+1} + M_{i+1}\vec{p}_{i\to i+1});\ \vec{s}_n^{\,*} = \vec{0}, \tag{3}$$

where ${}^i\mathbf{R}_{i+1}$ is the 3×3 rotation matrix representing D-H frame $i+1$ in frame i, $\vec{s}_\ell$ is the first-moment-of-inertia vector for link ℓ referred to and expressed in its own D-H frame, and $\vec{p}_{i\to\ell}$ is the vector from the origin of D-H frame i to the origin of frame ℓ and expressed in frame ℓ.

Let

$$u_{i,1} = \hat{z}_{i-1} \cdot (\vec{g} \times \vec{s}_{i-1}^{\,*}) \tag{4}$$

and

$$u_{i,2} = (\vec{s}_{i-1}^{\,*} \times \hat{z}_{i-1}) \cdot (\hat{z}_{i-1} \times \vec{g}), \tag{5}$$

where $\vec{g}$ is the upward-pointing gravity vector and $\hat{z}_i$ is the z axis of frame ℓ. Then, provided neither $\vec{s}_{i-1}^{\,*}$ nor $\vec{g}$ is parallel to $\hat{z}_{i-1}$, $u_{i,1}$ and $u_{i,2}$ allow the swing angle to be calculated as

$$\hat{\theta}_i = \text{Atan2}[u_{i,1}, u_{i,2}], \tag{6}$$

where the range of Atan2 is $(-\pi, \pi]$. If either $\vec{s}_{i-1}^{\,*}$ or $\vec{g}$ is parallel to $\hat{z}_{i-1}$, all values of q_i give the same potential energy, and thus

$$\hat{\theta}_i = 0. \tag{7}$$

If $\vec{s}_{i-1}^{\,*}$ or $\vec{g}$ is parallel to $\hat{z}_{i-1}$ or $\hat{\theta}_i = \pi$, the gradient of $\hat{\theta}_i$ is either $\mathbf{0}$ or undefined. Otherwise, from (6), the entries of $\nabla\hat{\theta}_i$ are calculated as follows:

$$\frac{\partial\hat{\theta}_i}{\partial q_j} = \frac{1}{u_{i,1}^2 + u_{i,2}^2}\left(\frac{\partial u_{i,1}}{\partial q_j}u_{i,2} - \frac{\partial u_{i,2}}{\partial q_j}u_{i,1}\right). \tag{8}$$

Methods for calculating $\frac{\partial u_{i,1}}{\partial q_j}$ and $\frac{\partial u_{i,2}}{\partial q_j}$ are given in English and Maciejewski (1998).

2.2. Dynamics at Low Velocities

Inherent in the definition of the swing angle $\hat{\theta}_i$ is the requirement that the joints excluding joint i be stationary. In much of the remainder of this paper, the swing angle will be applied to a moving manipulator as an approximation. We now discuss the quality of this approximation.

For a viscous-friction model, the differential equation governing the motion of the arm is expressed as

$$\tau = \mathbf{M}(\mathbf{q})\,\ddot{\mathbf{q}} + \mathbf{C}(\mathbf{q}, \dot{\mathbf{q}})\,\dot{\mathbf{q}} + \mathbf{V}(\mathbf{q})\dot{\mathbf{q}} + \mathbf{g}(\mathbf{q}). \tag{9}$$

Here, τ is the vector of applied joint torques; $\mathbf{M}(\mathbf{q})$ is the manipulator inertia matrix; $\mathbf{C}(\dot{\mathbf{q}}, \mathbf{q})$ is the matrix specifying centrifugal and Coriolis effects, each row i of which has the form $\dot{\mathbf{q}}^T \mathbf{C}_i(\mathbf{q})$; $\mathbf{V}(\mathbf{q})$ is the viscous-friction matrix; and $\mathbf{g}(\mathbf{q})$ is the vector of joint torques due to gravity. It is assumed that the manipulator's control law (feedback through τ) allows accurate tracking of a prescribed trajectory for the healthy joints.

Let joint i be free swinging, and let ϵ_i be defined such that

$$q_i = \hat{\theta}_i|_{q_i=0} + \epsilon_i. \tag{10}$$

Then, assuming the healthy joints are stationary, (9) gives, through entry i of the vector equation,

$$0 = M_{ii}\ddot{\epsilon}_i + V_{ii}(\epsilon_i)\dot{\epsilon}_i + \|\vec{s}^{\,*}_{i-1} \times \hat{z}_{i-1}\|\|\hat{z}_{i-1} \times \vec{g}\| \sin(\epsilon_i), \tag{11}$$

where the following were used: $\tau_i = 0$ (because joint i is free swinging), M_{ii} is not a function of ϵ_i, and entry i, i of $\mathbf{C}_i$ is zero. If joint i is free swinging with the motor engaged, M_{ii} and V_{ii} should reflect the motor inertia and friction. Equation (11) is an approximation for a slow-moving arm—provided ϵ_i and its first and second derivatives are bounded, the disturbance to (11) can be made arbitrarily small by time scaling the trajectory of the healthy joints. If $|\epsilon_i|$ is assumed small and V_{ii} changes little with ϵ_i, then (11) can be approximated by the following normalized linear differential equation:

$$0 \approx \ddot{\epsilon}_i + \frac{V^*_{ii}}{M_{ii}}\dot{\epsilon}_i + \frac{1}{M_{ii}}\|\vec{s}^{\,*}_{i-1} \times \hat{z}_{i-1}\|\|\hat{z}_{i-1} \times \vec{g}\|\epsilon_i, \tag{12}$$

where V^*_{ii} is the nominal value. Note that $M_{ii} \neq 0$ because $\mathbf{M}$ is positive definite. This system acts as one under a proportional plus derivative control law driving ϵ_i to zero (and therefore q_i to $\hat{\theta}_i|_{q_i=0}$). It has a damping ratio ζ, undamped natural frequency ω_n, and time constant τ_c given by the following:

$$\zeta = \frac{V^*_{ii}}{2\sqrt{M_{ii}\|\vec{s}^{\,*}_{i-1} \times \hat{z}_{i-1}\|\|\hat{z}_{i-1} \times \vec{g}\|}} \tag{13}$$

$$\omega_n = \sqrt{\frac{1}{M_{ii}}\|\vec{s}^{\,*}_{i-1} \times \hat{z}_{i-1}\|\|\hat{z}_{i-1} \times \vec{g}\|} \tag{14}$$

$$\tau_c = 2\frac{M_{ii}}{V^*_{ii}}. \tag{15}$$

Provided the manipulator's motion is slow enough that the disturbance to (12) is minimal, q_i can be viewed as tracking $\hat{\theta}_i|_{q_i=0}$ in much the same way as the healthy joints can be viewed as tracking their desired values. If fast motion of the arm (relative to τ_c) is desired, for large ζ, joint i will tend to lose tracking and lag behind, and for small ζ, the joint will tend to oscillate. However, even if this occurs, the arm can be stopped at key points and allowed to settle. Very fast motion may invalidate (11) and marginalize the usefulness of it (and, therefore, (12)) in predicting behavior.

2.3. Experimental Validation

To provide experimental confirmation for the above derivations, the simple three-axis mechanism shown in Figure 2 was constructed. It serves to validate that one can manufacture a manipulator that operates in both a locked-joint mode and a viscous-friction free-swinging mode. The mechanism contains two free-swinging joints that are actuated only with simple brakes. These joints are also equipped with encoders; however, the encoders are used only for data collection, not for the control of the free-swinging motion.

To evaluate the accuracy of the simple linearized dynamic model given by (12), an experiment was performed in which one of the free-swinging joints was manually moved to approximately 25 degrees from its lowest potential value (i.e., $\epsilon = 25$ degrees) and then released. This experiment was performed repeatedly with the position of the joint recorded every 100 ms. The resulting joint motions are presented in Figure 3, which shows the average over all trials and the maximum and minimum joint values for every time sample. These results show that the dynamic behavior of the free-swinging joint is quite consistent and thus could be approximated with an appropriate dynamic model. The best linear second-order model (i.e., the viscous-friction-based model given in (12)) is also shown in Figure 3. While the 25-degree initial configuration strains the small-angle linear approximation, (12) clearly represents a reasonable approximation to the behavior of the free-swinging joint. It is particularly accurate with respect to modeling the frequency of the resulting oscillations but less so with respect to the magnitude. This faster damping of the oscillations in the free-swinging joint is probably due to the unmodeled Coulomb friction and results in the arm settling after 4 seconds as opposed to the 6 seconds predicted by the model.

The most important aspect of the free-swinging joint motion is the accuracy to which it settles to its minimum potential value (i.e., the value of $\epsilon(t = \infty)$). Over the 100 trials that were performed, the average value of ϵ once the joint had settled (i.e., after 4 seconds) was on the order of 0.003 degrees with a standard deviation of 0.104 degrees (see Table 1). This demonstrates the feasibility of ignoring the high-speed

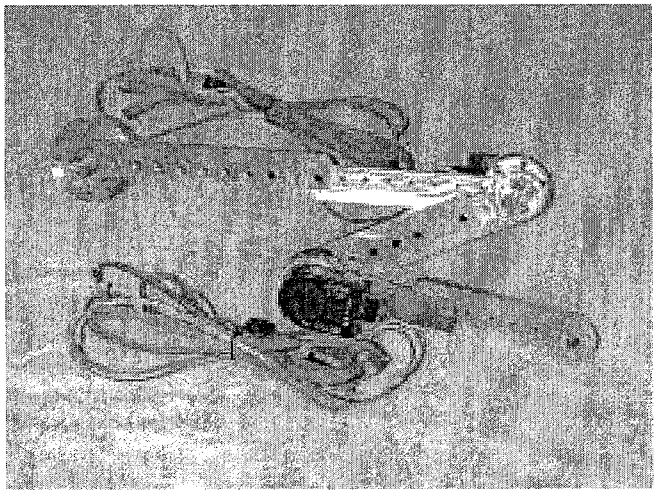

Fig. 2. A simple three-axis mechanism used to validate the simplified viscous-friction-based dynamic model.

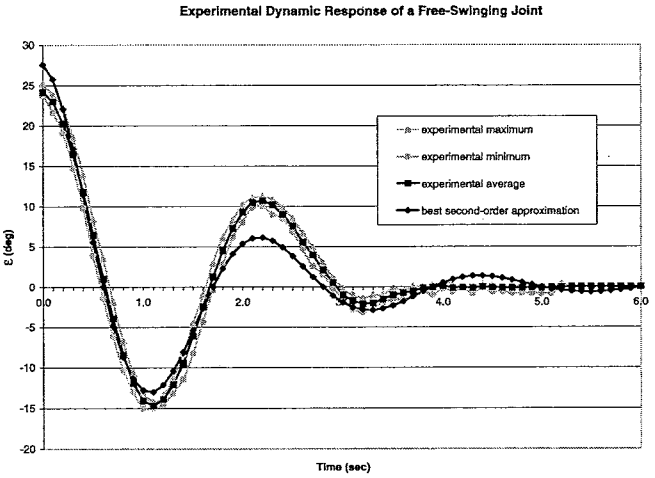

Fig. 3. Experimental dynamic response of a free-swinging joint.

Table 1. Repeatability of Swing Angle Convergence (100 trials)

$\arcsin \|\hat{z}_{i-1} \times \hat{\bar{g}}\|$	Ave. $\epsilon(\infty)$	Std. Dev. $\epsilon(\infty)$
15 deg	0.016 deg	0.123 deg
30 deg	0.003 deg	0.104 deg

dynamics of the free-swinging joint and simply stopping the motion of all joints for 4 seconds prior to applying the brakes on the free-swinging joint.

The accuracy of predicting both the transient behavior and the steady-state value of a free-swinging joint are clearly influenced by the amount of friction, the associated mass, and the angle between the free-swinging joint axis and the gravity vector. The most problematic of these three factors is the friction, since the unmodeled Coulumb friction can result in large steady-state values for ϵ. Somewhat surprisingly, the angle between the free-swinging joint axis and the gravity vector does not appreciably affect the steady-state value of ϵ. Even for free-swinging joint axes that are only 15 degrees from vertical, the standard deviation of $\epsilon(\infty)$ is only 0.123 degrees (see Table 1). Thus, robot designs that are typically mounted with joint axes parallel to gravity (e.g., SCARA robots) would only need to be moderately tilted in order to utilize free-swinging behavior.

3. Single-Mode Kinematics

Prior to focusing on the process of switching modes, in this section, kinematic methods will be presented for postfailure control in the presence of a single mode of failure.

For a healthy arm, the positional-kinematic equation by which a manipulator configuration reaches a hand pose $\mathbf{T}_{\text{hand}}$ is given by

$$f(\mathbf{q}) = \mathbf{T}_{\text{hand}}, \tag{16}$$

where $f(\cdot)$ is the mapping from configuration to hand pose. Because (16) is typically difficult to solve, a linearization is often made based on the manipulator Jacobian equation. If $\dot{\mathbf{x}}$ is a representation of the hand's linear and/or rotational velocity and the corresponding manipulator Jacobian is given by

$$\mathbf{J} = [\mathbf{j}_1\ \mathbf{j}_2\ \cdots\ \mathbf{j}_n], \tag{17}$$

then the manipulator Jacobian equation is

$$\dot{\mathbf{x}} = \mathbf{J}\dot{\mathbf{q}}. \tag{18}$$

For solving (18) given a desired $\dot{\mathbf{x}}$, one can apply any number of techniques using a suitable joint-rate weighting matrix (English and Maciejewski 2000b). This weighting matrix will be labeled $\mathbf{W}(\mathbf{q})$—it is symmetric and if positive definite defines a metric on the $\dot{\mathbf{q}}$ space through

$$\eta(\dot{\mathbf{q}}) = \sqrt{\dot{\mathbf{q}}^T \mathbf{W} \dot{\mathbf{q}}}. \tag{19}$$

Different modes of failure in this system will be addressed below, and their impact on these equations will be discussed.

3.1. Locked Joint

Assume a failure at joint i. When the failed joint is locked, a manipulator configuration that reaches hand pose $\mathbf{T}_{\text{hand}}$ must satisfy (16) and

$$q_i = \ell_i, \tag{20}$$

where ℓ_i is the locked value. The velocity equation becomes

$$\dot{\mathbf{x}} = {}^{i}\mathbf{J}\,{}^{i}\dot{\mathbf{q}}, \tag{21}$$

where ${}^i\mathbf{J}$ is formed by removing column i from $\mathbf{J}$, that is,

$$ {}^i\mathbf{J} = [\mathbf{j}_1 \ \cdots \ \mathbf{j}_{i-1} \ \mathbf{j}_{i+1} \ \cdots \ \mathbf{j}_n], \tag{22} $$

and ${}^i\mathbf{q}$ is formed by removing element i from $\mathbf{q}$. For trajectory generation, (21) can be solved for ${}^i\dot{\mathbf{q}}$, which can be integrated to find ${}^i\mathbf{q}$ while q_i remains constant.

The induced weighing matrix for ${}^i\dot{\mathbf{q}}$ is ${}^i\mathbf{W}$, formed by removing row i and column i from $\mathbf{W}$. Clearly, ${}^i\dot{\mathbf{q}}^T {}^i\mathbf{W} {}^i\dot{\mathbf{q}} = \dot{\mathbf{q}}^T\mathbf{W}\dot{\mathbf{q}}$ when q_i is constant. If $\mathbf{W}$ is positive definite, then ${}^i\mathbf{W}$ is also.

3.2. *Free-Swinging Joint*

When joint i is in free-swinging mode, the manipulator configuration to reach a hand pose $\mathbf{T}_{\text{hand}}$ while stationary must satisfy (16) and

$$ \hat{\theta}_i(\mathbf{q}) = 0, \tag{23} $$

where $\hat{\theta}_i$ is the swing angle.

For a slow-moving manipulator, $\dot{\hat{\theta}}_i(\mathbf{q}) \approx 0$. Provided neither $\vec{s}^*_{i-1}$ nor $\vec{g}$ is parallel to $\hat{z}_{i-1}$, this gives, since element i of $\nabla\hat{\theta}_i$ is -1,

$$ \dot{q}_i \approx {}^i\dot{\mathbf{q}}^T {}^i\nabla\hat{\theta}_i, \tag{24} $$

where ${}^i\nabla\hat{\theta}_i$ equals $\nabla\hat{\theta}_i$ with entry i removed.

The velocity equation for a slow-moving manipulator then becomes

$$ \dot{\mathbf{x}} \approx {}^i\hat{\mathbf{J}} \, {}^i\dot{\mathbf{q}}, \tag{25} $$

where

$$ {}^i\hat{\mathbf{J}} = {}^i\mathbf{J} + \mathbf{j}_i {}^i\nabla\hat{\theta}_i{}^T. \tag{26} $$

Thus, when the manipulator is slow moving, the velocity equation's structure for a free-swinging failure in (25) is the same as that for a locking failure in (21). The difference between the locked-joint and the free-swinging Jacobians is the rank-one matrix $\mathbf{j}_i {}^i\nabla\hat{\theta}_i{}^T$. For trajectory generation, (25) can be solved for ${}^i\dot{\mathbf{q}}$, which can be integrated to find ${}^i\mathbf{q}$. An updated value of ${}^i\mathbf{q}$ can then be used with the previous value of q_i to solve for the associated swing angle to be added to the previous value of q_i to obtain the new value.

The weighing matrix induced by a free-swinging failure is

$$ {}^i\hat{\mathbf{W}} = {}^i\mathbf{W} + W_{ii} {}^i\nabla\hat{\theta}_i \, {}^i\nabla\hat{\theta}_i{}^T + {}^i\mathbf{W}_i {}^i\nabla\hat{\theta}_i{}^T + {}^i\nabla\hat{\theta}_i {}^i\mathbf{W}_i^T, \tag{27} $$

where W_{ii} is diagonal entry i of $\mathbf{W}$ and ${}^i\mathbf{W}_i$ is column i of $\mathbf{W}$ with entry i removed. With this definition, ${}^i\dot{\mathbf{q}}^T {}^i\hat{\mathbf{W}} {}^i\dot{\mathbf{q}} \approx \dot{\mathbf{q}}^T\mathbf{W}\dot{\mathbf{q}}$ when q_i is free swinging. As was the case for ${}^i\mathbf{W}$, if $\mathbf{W}$ is positive definite, then ${}^i\hat{\mathbf{W}}$ is also.

4. Switching between Modes

A locked-joint failure cannot be arbitrarily converted to a free-swinging failure without undesirable dynamic effects. Equation (25) does not apply when the swing angle is large because acceleration- and Coriolis-based forces are manifest and the joint swings, possibly violently. Thus, the primary issue when making this type of conversion is ensuring that the swing angle is at (or at least near) zero.

Conversely, when the manipulator is operating in free-swinging mode and is slow moving, a brake can be applied at any time with minimal dynamic effects. Thus, (25) can be converted to (21) whenever ${}^i\hat{\mathbf{J}}$ presents undesirable properties. The important parameter when this type of conversion is made is the actual value of q_i—it will be frozen until another conversion. Thus, the primary issue for a free-swinging-to-locked conversion is setting the value of the failed joint.

These two issues of setting the swing angle to zero in a locked-joint manipulator and setting the joint angle to a desired value in a free-swinging manipulator are in fact the same positional kinematic problem—finding a configuration giving both $\hat{\theta}_i = 0$ and $q_i = \ell_i$ for some ℓ_i. It will be shown here that for a slow-moving manipulator, they are amenable to the same form of velocity-kinematic equation.

4.1. *Locked to Free Swinging*

Because this type of conversion should be made when the value of the swing angle is zero, the focus here is on finding a configuration of the failed, locked-joint manipulator that gives a vanishing swing angle. If the arm's dynamic and kinematic parameters are well-known, this is essentially a root-finding problem for which any number of techniques can be applied.

Here, the problem will be cast as a familiar velocity-kinematic equation. This has the advantage of general applicability and quality, if not completeness, of its solution. It can be used with feedback from sensors to refine solutions when the arm's parameters are in doubt.

When joint i is locked, the governing velocity-kinematic equation is given by

$$ \dot{\hat{\theta}}_i = {}^i\nabla\hat{\theta}_i{}^T {}^i\dot{\mathbf{q}}. \tag{28} $$

Values of ${}^i\dot{\mathbf{q}}$ for control can be found in a number of ways, with possible inclusion of additional constraints. General methods for finding joint rates to solve the Jacobian equation given in (18) (Liégeois 1977; English and Maciejewski 2000b) can be directly applied to (28).

For example, one approach is to use a weighted pseudoinverse based on ${}^i\mathbf{W}$. This allows $\hat{\theta}_i$ to be differentially changed with the minimum joint-rate measure as given by (19). If ${}^i\mathbf{W}$ is positive definite and provided ${}^i\nabla\hat{\theta}_i \neq \mathbf{0}$, this solution for a desired value of $\dot{\hat{\theta}}_i$ can be found as follows:

$$ {}^{i}\dot{\mathbf{q}} = \frac{\dot{\hat{\theta}}_i}{{}^{i}\nabla\hat{\theta}_i^{T}\,{}^{i}\mathbf{W}^{-1}\,{}^{i}\nabla\hat{\theta}_i}\,{}^{i}\mathbf{W}^{-1}\,{}^{i}\nabla\hat{\theta}_i. \tag{29} $$

Equation (29) can be used with torque feedback to set the swing angle accurately to zero. The swing angle can be found for small values ($-\frac{\pi}{2} \leq \hat{\theta}_i \leq \frac{\pi}{2}$) using

$$ \hat{\theta}_i = \sin^{-1}\left(\frac{-g_i}{\|\vec{s}_{i-1}^{\,*} \times \hat{z}_{i-1}\|\,\|\hat{z}_{i-1} \times \vec{g}\|}\right), \tag{30} $$

where g_i is the measured torque at joint i.

4.2. Free Swinging to Locked

The primary goal for this type of conversion is to lock the joint at the appropriate value. Therefore, the focus is on seeking a configuration of the failed, free-swinging manipulator that gives the desired value of the failed joint. The velocity-kinematic equation for this focus is

$$ \dot{q}_i \approx {}^{i}\nabla\hat{\theta}_i^{T}\,{}^{i}\dot{\mathbf{q}}, \tag{31} $$

which can be directly used with measured joint position feedback. It has the same form of solution as did the locked-to-free-swinging conversion. Therefore, again as an example, if ${}^{i}\hat{\mathbf{W}}$ is positive definite and provided ${}^{i}\nabla\hat{\theta}_i$ is defined and not equal to zero, a healthy joint-rate solution giving a desired value of $\dot{q}_i$ can be found using

$$ {}^{i}\dot{\mathbf{q}} = \frac{\dot{q}_i}{{}^{i}\nabla\hat{\theta}_i^{T}\,{}^{i}\hat{\mathbf{W}}^{-1}\,{}^{i}\nabla\hat{\theta}_i}\,{}^{i}\hat{\mathbf{W}}^{-1}\,{}^{i}\nabla\hat{\theta}_i. \tag{32} $$

5. Global Issues

An important global issue is finding the postfailure workspace when failure mode switching is possible. Defining the workspace can be difficult even for healthy joints, however, and the focus of this section will be on finding the range of possible values of the failed joint.

In addition to establishing what values of the failed joint are achievable, this section will present a global approach to placing the failed joint at a particular value. The kinematic equations and methods in Section 4 were ideal for using feedback for fine control and represented a general approach to finding desired configurations. However, they are local methods and cannot always find a solution. This shortcoming will be addressed here.

5.1. Postfailure Workspace

For a stationary manipulator, let the set of all values obtainable by q_i while in free-swinging mode be defined as $\mathcal{K}_i$, and let $\{\mathcal{K}_i^k\}$ be the set of segments such that

$$ \mathcal{K}_i = \bigcup_{j=1}^{N_i} \mathcal{K}_i^j, \tag{33} $$

where $\{\mathcal{K}_i^k\}$ has the smallest cardinality. Then, for all configurations with $\hat{\theta}_i = 0$ where q_i is an endpoint of the segment $\mathcal{K}_i^j$, either (a) $\dot{q}_i$ is directly constrained through

$$ q_i = q_i^{+} \tag{34} $$

or

$$ q_i = q_i^{-}, \tag{35} $$

where q_i^{-} and q_i^{+} are the lower and upper joint position limits, respectively, of joint i, or (b) $\dot{q}_i$ as given through (31) is indirectly constrained in that one of the following must be true for every $k \neq i$:

$$ \nabla\hat{\theta}_{i,k} \text{ is undefined} \tag{36} $$

$$ \nabla\hat{\theta}_{i,k} = 0 \tag{37} $$

$$ q_k = q_k^{+} \tag{38} $$

$$ q_k = q_k^{-}, \tag{39} $$

where $\nabla\hat{\theta}_{i,k}$ is entry k of $\nabla\hat{\theta}_i$. Additionally, for r_k defined as

$$ \begin{aligned} r_k(q_k) &= \nabla\hat{\theta}_{i,k} \quad q_k = q_k^{+} \\ &= -\nabla\hat{\theta}_{i,k} \quad q_k = q_k^{-} \\ &= 0 \quad \text{otherwise,} \end{aligned} \tag{40} $$

if neither (34) nor (35) applies, one of the following must be true:

$$ r_k(q_k) \geq 0, \ \forall k \tag{41} $$

$$ r_k(q_k) \leq 0, \ \forall k. \tag{42} $$

Otherwise, it would be possible to move the healthy joints to either increase or decrease the value of the failed joint.

Thus, $\mathcal{K}_i$ can be established by first finding the typically finite number of values satisfying the above conditions. These can then be used to find the actual endpoints using second-order (or higher if necessary) conditions with the joint-limit constraints. For example, as a second-order condition, when no joints are at their limits, ${}^{i}\mathbf{H}(\hat{\theta}_i)$ must be nonindefinite, where ${}^{i}\mathbf{H}(\hat{\theta}_i)$ is the Hessian of $\hat{\theta}_i$ with column i and row i removed.

5.2. Setting the Failed Joint

If a desired value of q_i is known to be an element of $\mathcal{K}_i$ and cannot be obtained using the local methods given in Section 4, a global approach must be used, at least to define a starting point for fine control with the local methods. Often, simple algorithms based on sets of differential equations or even closed-form equations can be used to guarantee a solution. Alternatively, manipulator configurations giving $\mathcal{K}_i$ to some level of discretization can be tabulated, which can be done quite efficiently. For example, for a seven-joint manipulator, if each $\mathcal{K}_i$ comprises all joint values (the worst case) and all $\mathcal{K}_i$ are discretized by 1-degree increments, only $360 \times 6 \times 7 = 15,120$ joint values will need to be stored to ensure all values of all joints can be reached to within one-half of 1 degree after any joint failure. (This assumes that a collision-free path can be found between the current configuration and the tabulated configuration.)

A starting point for finding the tabulated values is to begin with the segment endpoints established using the conditions in Section 5.1 and drive away from them using a gradient method (a second-order method can be used for the first step). The holes left after exhausting this approach can be filled using a numerical nonlinear equation-solving algorithm or a polynomial root-finding method. Because this tabulation is performed off-line, computational speed is much less of a concern.

6. Examples

6.1. Planar Examples

For these examples, the same planar arm as was shown in Figure 1 will be used to explore the postfailure workspace, switching strategies, and operation in the free-swinging mode.

The example planar manipulator's link lengths are 1 m, the link masses are 10 kg, and the center of mass of each link is at the center of the link. The link inertias are modeled as thin rods; that is, the second moment of inertia of each link about its center is given by

$$\mathbf{J}^{\mathrm{cm}} = \begin{bmatrix} 0 & 0 & 0 \\ 0 & \frac{5}{6} & 0 \\ 0 & 0 & \frac{5}{6} \end{bmatrix}. \tag{43}$$

The joint angles q_i will be measured counterclockwise, with a right-horizontal reference position for joint one and in-line reference positions for joints two and three. All joints can assume any value. The task will be end-effector positioning only (i.e., orientation is not considered), and thus the manipulator has 1 degree of kinematic redundancy when fully operational.

6.1.1. Postfailure Workspaces

This manipulator has full range of motion in all three joints, so from the conditions of Section 5.1, the endpoints of the sets of achievable postfailure values must satisfy (a) $\hat{\theta}_i = 0$, (b) ${}^i\nabla\hat{\theta}_i = \mathbf{0}$ or undefined, and (c) nonindefinite ${}^i\mathbf{H}(\hat{\theta}_i)$.

For the various swing angles not equal to π, the reduced gradients are given by

$${}^1\nabla\hat{\theta}_1 = \begin{bmatrix} \frac{-10-15\cos(q_2)-6\cos(q_3)-5\cos(q_2+q_3)}{35+30\cos(q_2)+6\cos(q_3)+10\cos(q_2+q_3)} \\ \frac{-1-3\cos(q_3)-5\cos(q_2+q_3)}{35+30\cos(q_2)+6\cos(q_3)+10\cos(q_2+q_3)} \end{bmatrix} \tag{44}$$

$${}^2\nabla\hat{\theta}_2 = \begin{bmatrix} -1 \\ \frac{-1-3\cos(q_3)}{10+6\cos(q_3)} \end{bmatrix} \tag{45}$$

$${}^3\nabla\hat{\theta}_3 = \begin{bmatrix} -1 \\ -1 \end{bmatrix}. \tag{46}$$

Because (45) and (46) are always defined and nonzero, there can be no endpoints to the joint two and joint three achievable sets $\mathcal{K}_2$ and $\mathcal{K}_3$. And because the sets are clearly not empty, the implication is that all angle values are achievable after a failure. Thus, the postfailure range of controllable motion for joints two and three is identical to the range of a healthy manipulator.

For the joint one case, however, the reduced gradient in (44) can become zero. Setting ${}^1\nabla\hat{\theta}_1 = 0$ yields four real solution sets for $\{q_2, q_3\}$: $\{\tan^{-1}(\frac{\sqrt{21}}{2}) - \pi, \pi\}$, $\{\pi - \tan^{-1}(\frac{\sqrt{21}}{2}), \pi\}$, $\{\tan^{-1}(\frac{3}{4}) - \pi, 0\}$, and $\{\pi - \tan^{-1}(\frac{3}{4}), 0\}$. The first two angle sets give an indefinite Hessian and therefore cannot correspond to endpoints. The third angle set yields a negative definite ${}^1\mathbf{H}(\hat{\theta}_1)$, and the fourth yields a positive definite ${}^1\mathbf{H}(\hat{\theta}_1)$. Thus, the third angle set will give the upper bound and the fourth the lower bound for $\mathcal{K}_1$. Using these in

$$\begin{aligned} \hat{\theta}_1 = \mathrm{Atan2}[&-(5\cos(q_1) + 3\cos(q_1 + q_2) \\ &+ \cos(q_1 + q_2 + q_3)), -(5\sin(q_1) \\ &+ 3\sin(q_1 + q_2) + \sin(q_1 + q_2 + q_3))] \end{aligned} \tag{47}$$

to solve for $q_1 = \hat{\theta}_i|_{q_1=0}$ gives the set of postfailure achievable values as $q_1 \in \mathcal{K}_1 = [\tan^{-1}(\frac{3}{4}) - \pi, -\tan^{-1}(-\frac{3}{4})]$. The union of all radius-two circles centered at $\{\cos(q_1), \sin(q_1)\}$ over this range gives the postfailure workspace when switching is possible. The switching postfailure workspaces are shown along with the worst-case postfailure workspaces for locking and free-swinging failures in Figure 4.

6.1.2. Switching Strategy

In this section, a strategy for postfailure operation through switching will be illustrated. The failure will lie in joint one.

The beginning configuration is the top one from the right-hand side of Figure 1. The goal is to reach the point $\{-2.5, 0\}$. To achieve this, it is necessary to use a mode-switching scheme. To reach $\{-2.5, 0\}$, q_1 must be greater than $\cos^{-1}(-\frac{13}{20})$ and less than $\pi - \cos^{-1}(-\frac{13}{20})$. The intersection of this range of values with $\mathcal{K}_1$ as found above gives $\tan^{-1}(\frac{3}{4}) \leq q_i \leq \pi - \cos^{-1}(-\frac{13}{20})$.

The joint-rate weighting matrix is given by

$$\mathbf{W} = \begin{bmatrix} 9 & 0 & 0 \\ 0 & 4 & 0 \\ 0 & 0 & 1 \end{bmatrix}. \tag{48}$$

This is an appropriate choice for reducing the relative burden on the inboard joints. A switching sequence based on using (48) in (29) and (32) for moving q_1 and relocking it in this range to achieve the task is shown in Figure 5.

6.1.3. Joint Trajectory Generation

In this section, postfailure operation through joint trajectory generation will be explored. The failure for this example lies in joint one. The joint one swing angle is given by (47), and, provided $\hat{\theta}_1 \neq \pi$, the gradient is given by

$$\nabla\hat{\theta}_1 = \begin{bmatrix} -1 \\ \frac{-10-15\cos(q_2)-6\cos(q_3)-5\cos(q_2+q_3)}{35+30\cos(q_2)+6\cos(q_3)+10\cos(q_2+q_3)} \\ \frac{-1-3\cos(q_3)-5\cos(q_2+q_3)}{35+30\cos(q_2)+6\cos(q_3)+10\cos(q_2+q_3)} \end{bmatrix}. \tag{49}$$

The motor is assumed to be disconnected from the failed joint for this simulation experiment, so M_{ii} does not include the motor inertia and V_{ii} does not include the motor friction. This would be appropriate for a failure occurring, for example, between the gears and the joint. Here, M_{ii} is the diagonal entry of the mass matrix induced by the inertia of the manipulator's links, and it is assumed that $V_{ii} = 15.0$.

A trajectory was generated using the method given in Section 3.2 for an end-effector path given by the line segment from $(-0.75, -2.0, 0.0)$ to $(-0.75, 0.0, 0.0)$. This is the path shown in Figure 1, and it lies well within the joint one free-swinging postfailure workspace as shown in Figure 4. To form an endpoint trajectory from this path, a trapezoidal velocity profile was used with a 20% speedup time and 20% slowdown time. Three configurations along the idealized joint path for this trajectory are shown on the left-hand side of Figure 1. For this joint path, $\zeta \in [0.046, 0.145]$ and $\omega_n \in [2.40, 3.08]$ both start at the low end and finish at the high end of their ranges. Thus, the system would be expected to be underdamped and oscillate with 2.0 to 2.6 seconds per cycle (with the lower value at the end of the trajectory). And this is in fact what is seen in dynamic simulations. The error in joint one for four trajectory times is illustrated in Figures 6 and 7.

6.2. Spatial Examples

In this section, the example manipulator is a Robotics Research Corporation K-1207i as shown in Figure 8. Its D-H parameters (based on the labeling scheme of Paul 1981) are given in Table 2, the software joint limits are given in Table 3, and the link masses and centers of mass are given in Table 4. The upward-pointing gravity vector is $(9.8, 0, 0)$. The K-1207i has 1 degree of redundancy for the task of hand positioning and orienting.

6.2.1. Joint Four

As a straightforward case, this section investigates the postfailure capabilities of joint four.

In general, if the axis of a failed outboard joint i can be made parallel to the axis of a healthy inboard joint j, regardless of the values of q_i and q_j, provided neither $\vec{s}^*_{i-1}$ nor $\vec{g}$ is parallel to the axes, $\nabla\hat{\theta}_{i,j} = \pm 1$. Then, the conditions of (36) and (37) are not satisfied for any values of q_i and q_j. Under these conditions, if the values satisfying (38) and (39) lie outside the limits established by (34) and (35), $\mathcal{K}_i$ comprises all values of q_i within its normal joint limits and the postfailure workspace equals the healthy workspace.

This is in fact the case when we focus on joint four. Let the configuration of the arm be constrained to

$$\mathbf{q} = \begin{bmatrix} q_1 \\ -\frac{\pi}{2} \\ -\frac{\pi}{2} \\ q_4 \\ \pi \\ 0 \\ 0 \end{bmatrix}, \tag{50}$$

then, for example, when $q_1 = \frac{3\pi}{4}$, $q_4 = -2.58$ to give zero $\hat{\theta}_4$—this is the configuration shown in Figure 8. Under these conditions, the axis of joint four is parallel to the axis of joint one and $\frac{\partial}{\partial q_1}\hat{\theta}_4 = -1$.

Therefore, (36) and (37) are never satisfied for $k = 1$, leaving only (34), (35), (38), and (39). For the point $\{q_1, q_4\} = \{\frac{3\pi}{4}, -2.58\}$, the angular difference between q_4 and its upper limit (2.58) is less than the difference between q_1 and its lower limit (5.50), and the angular difference between q_4 and its lower limit (0.47) is less than the difference between q_1 and its upper limit (0.78). Therefore, the endpoints of $\mathcal{K}_4$ are the normal joint limits of q_4.

6.2.2. Joint Three

As a somewhat more involved case, this section investigates the postfailure capabilities of joint three. Let the configuration of the arm be constrained to

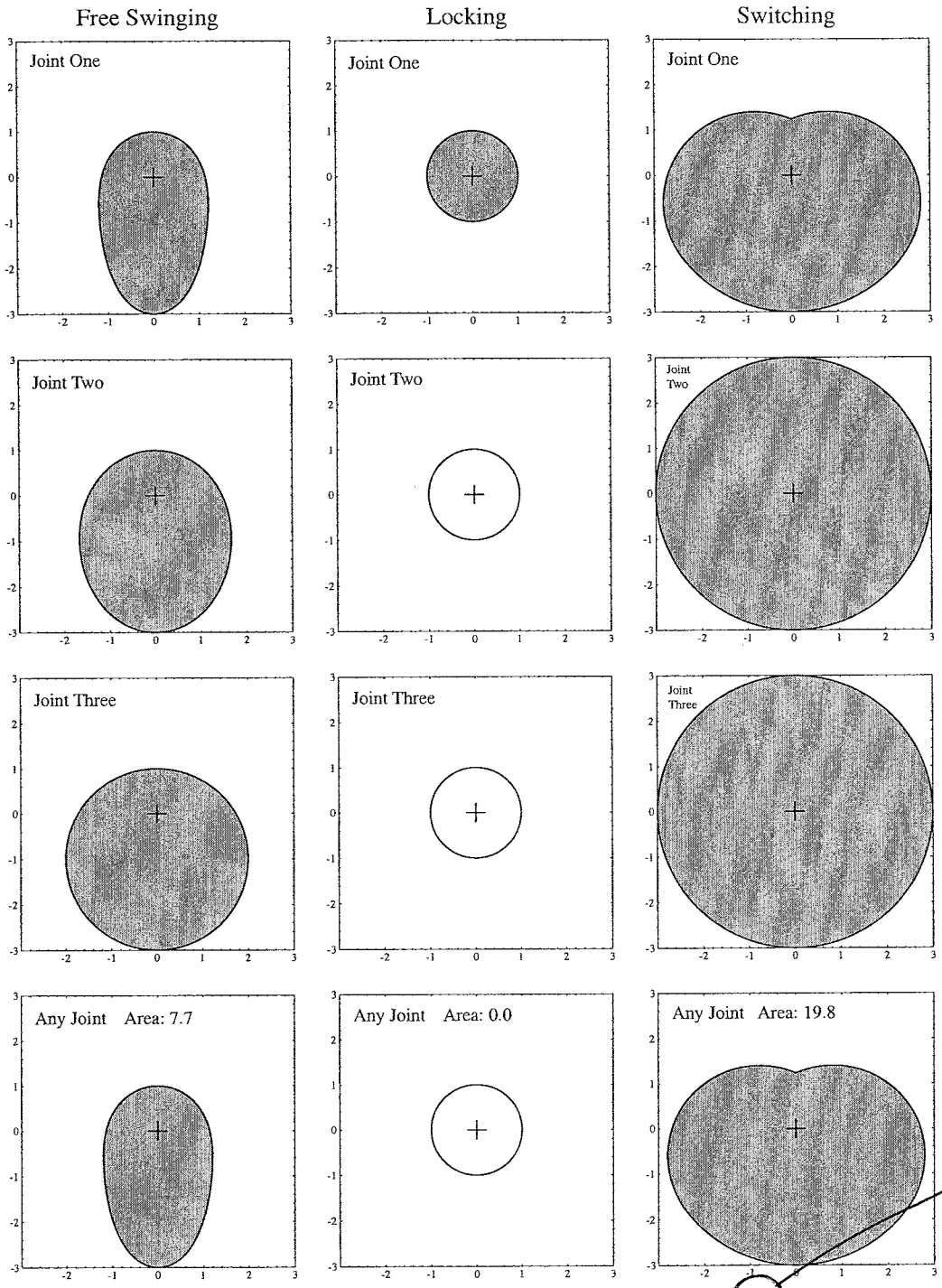

Fig. 4. Guaranteed postfailure workspaces of the example planar arm (as shown in Fig. 1) for free-swinging failures, for locking failures, and when switching is possible. The cases for each individual joint are shown as well as the case for any joint failure, which is the intersection of the three corresponding single-joint cases. The free-swinging workspaces were found using the method given in English and Maciejewski (1997). Significant improvement is made in all cases through switching. The areas of the free swinging, locking, and switching guaranteed postfailure workspaces for any joint are 7.7m^2, 0.0m^2, and 19.8m^2, respectively.

Table 2. D-H Parameters for the Robotics Research Corporation K-1207i

Link	a (m)	d (m)	α (rad)	θ (rad)
1	−0.1016	0.0000	−1.5708	q_1
2	0.1016	0.0000	1.5708	q_2
3	−0.0857	0.5461	−1.5708	q_3
4	0.0857	0.0000	1.5708	q_4
5	−0.0591	0.5461	−1.5708	q_5
6	0.0591	0.0000	1.5708	q_6
7	0.0000	0.1778	0.0000	q_7

Table 3. Joint Limits in Radians for the Robotics Research Corporation K-1207i

Joint	Upper Limit	Lower Limit
1	3.1410	−3.1410
2	−0.0543	−3.0510
3	0.0000	−6.2800
4	0.0000	−3.0510
5	6.2800	−6.2800
6	0.6100	−2.9670
7	6.2800	−6.2800

Table 4. Masses and Centers of Mass for the Robotics Research Corporation K-1207i

Link	Mass (kg)	c_x (m)	c_y (m)	c_z (m)
1	19.051	0.0000	0.0000	−0.0030
2	9.299	0.0000	0.0000	0.3239
3	11.113	0.0000	0.0000	0.0064
4	5.897	0.0000	0.0000	0.3200
5	4.536	0.0000	0.0000	0.0127
6	2.381	0.0000	0.0000	0.1219
7	0.325	0.0000	0.0000	−0.0200

$$\mathbf{q} = \begin{bmatrix} \sin(x) \\ \cos(x) - \frac{\pi}{2} \\ q_3 \\ -\frac{\pi}{2} \\ 0 \\ 0 \\ 0 \end{bmatrix}. \quad (51)$$

Then,

$$\frac{\partial}{\partial x}\hat{\theta}_3 = \frac{4\cos(x)\sin(\cos(x))+2\cos(\cos(x))\sin(x)\sin(2\sin(x))}{-3+\cos(2\cos(x))+\cos(2\sin(x))+\cos(2\cos(x))\cos(2\sin(x))}, \quad (52)$$

which is strictly negative (both terms in the numerator are always nonnegative and not zero simultaneously, and the denominator is strictly negative), and therefore either $\frac{\partial}{\partial q_1}\hat{\theta}_3 \neq 0$ or $\frac{\partial}{\partial q_2}\hat{\theta}_3 \neq 0$ for all x. Thus, neither (36) nor (37) can apply. By design, neither (38) nor (39) applies for any value of x. Therefore, only (34) or (35) can determine the endpoints of $\mathcal{K}_3$, and thus the postfailure achievable values of q_3 are the same as the prefailure achievable values.

6.2.3. Remaining Joints

For joints one, five, and six, methods similar to those used above can be used to establish that the postfailure achievable values for these joints also equal their prefailure values. For joint seven, because the first-moment-of-inertia vector $\vec{s}_6^*$ is always parallel to $\hat{z}_6$, the swing angle is always zero and $\mathcal{K}_7$ is empty. This could be easily remedied by shifting the center of mass of the last link away from the joint axis, enabling all values to be achieved after a failure—this is a straightforward manipulator design issue.

The most complicated case is that of joint two. Based on a numerical search of the conditions of Section 5.1, $\mathcal{K}_2$ is composed of a single segment with endpoints ${}^1\kappa_2^1 = -1.25$ and ${}^2\kappa_2^1 = -2.28$. The upper value can be reached with

$$\mathbf{q}_{\text{upper}} = [0, -1.25, -6.27, -2.15, 3.29, -0.70, 0]^T, \quad (53)$$

and the lower value can be reached with

$$\mathbf{q}_{\text{lower}} = [0, -2.28, -3.13, -2.54, 3.29, -0.70, 0]^T. \quad (54)$$

Configurations giving each of these are shown in Figure 9. Note a healthy joint path given by ${}^2\mathbf{q}_{\text{lower}} + \alpha({}^2\mathbf{q}_{\text{upper}} -$

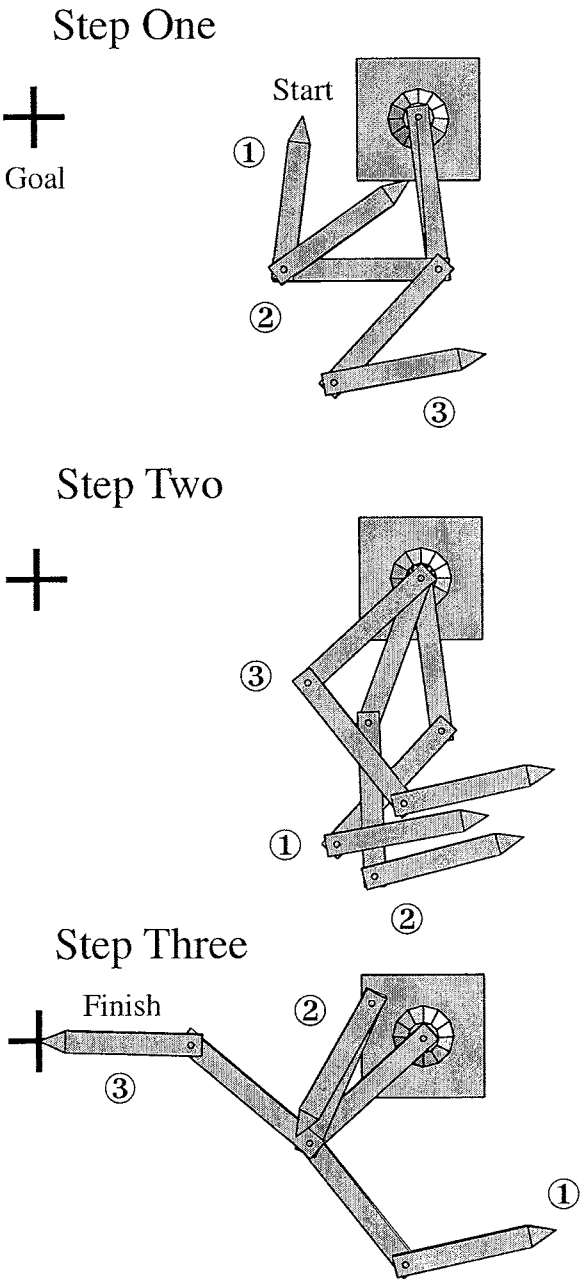

Fig. 5. Three configurations for each of three steps of a switching strategy are shown. The goal is to reach $\{-2.5, 0\}$, shown by crosshairs. In step one, the manipulator is moved with the brake engaged using (29) from its initial configuration to a configuration giving a zero swing angle, where the brake is released. In step two, the arm is moved using (32) to place joint one at the desired value, where the brake is reapplied. In the final step, the manipulator is moved to the desired hand position by solving (18) for joint rates that give straight-line endpoint motion.

(21)

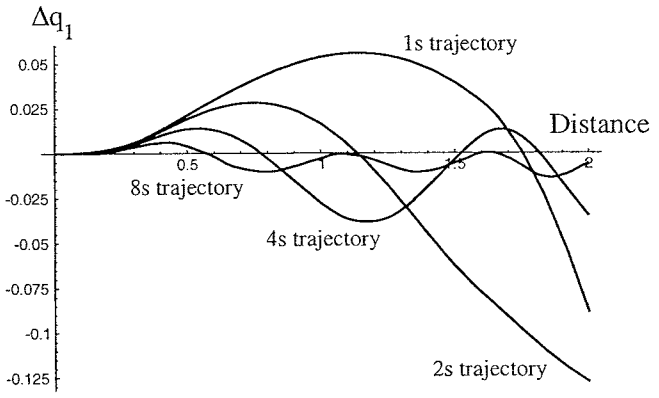

Fig. 6. Dynamically simulated joint one error as the arm traced the 2 m vertical trajectory shown in Figure 1 with joint one free swinging.

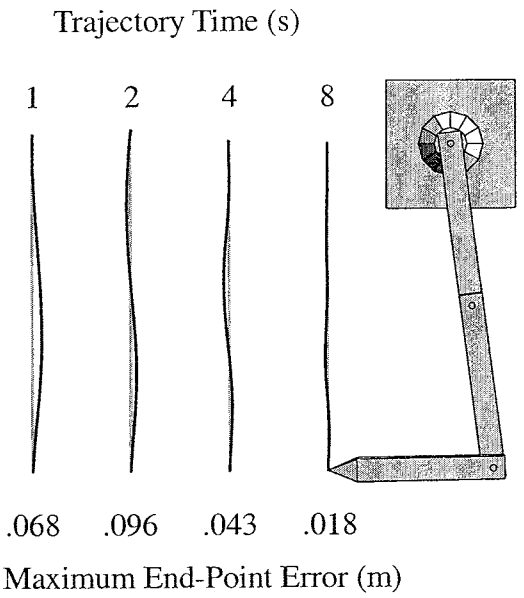

Fig. 7. Endpoint path for the trajectories generating Figure 6. The maximum endpoint error for each of the trajectory speeds is shown (this value includes both the horizontal and vertical error components). For reference, the arm at the start is shown for the 8-second trajectory.

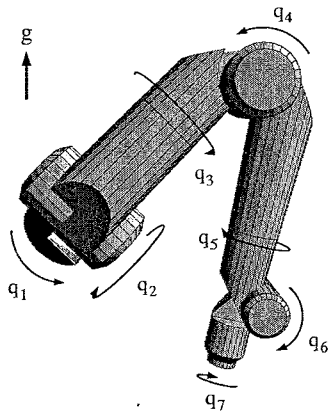

Fig. 8. Example spatial manipulator—the Robotics Research Corporation K-1207i. The arm has seven joints, as shown. The D-H parameters are given in Table 2, the joint limits are given in Table 3, and the masses and centers of mass are given in Table 4. Joint four is free swinging in this configuration.

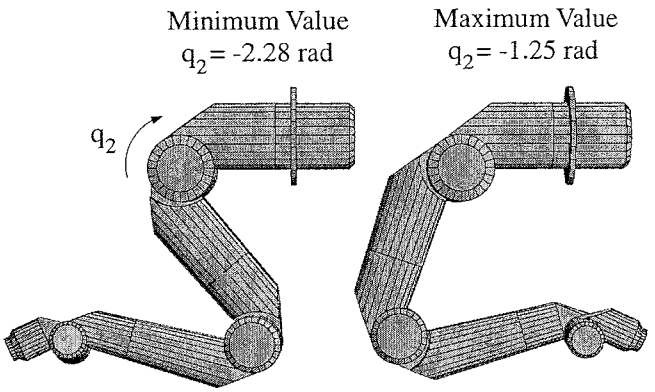

Fig. 9. As viewed from the side, the K-1207i in a configuration giving the minimum value of q_2 (left) and the maximum value of q_2 (right) after a failure. Most of the healthy joint displacement between the two configurations lies with joint three.

Table 5. Postfailure Joint Ranges for the Robotics Research Corporation K-1207i

Joint	Upper Limit	Lower Limit
1	3.1410	−3.1410
2	−1.2476	−2.2801
3	0.0000	−6.2800
4	0.0000	−3.0510
5	6.2800	−6.2800
6	0.6100	−2.9670
7	none	none

$^2\mathbf{q}_{\text{lower}}$) as parameterized by α will provide all possible values of q_2 and therefore can be used as a global technique. The complete set of achievable postfailure values is given in Table 5.

7. Summary

This paper presented ways to exploit a manipulator's postfailure capabilities when conversion between free-swinging and locked-joint failure modes is possible. Velocity control methods were discussed for both types of failures, and ways of effectively converting between the two types were presented. Also, analyses of global effects, including postfailure workspaces, were made, which provided a set of tools for manipulator design. Examples of switching strategies and postfailure operation were given.

Acknowledgments

The authors would like to gratefully acknowledge the contributions of Matthew R. Wortley, Sai Krishna Mallipeddi, and Kristin Lai-Fook, who manufactured and experimentally evaluated the free-swinging mechanism described in Section 2.3.

References

Arai, H., and Tachi, S. 1991a. Position control of a manipulator with passive joints using dynamic coupling. *IEEE Transactions on Robotics and Automation* 7:528–534.

Arai, H., and Tachi, S. 1991b. Position control system of a two degree of freedom manipulator with a passive joint. *IEEE Transactions on Industrial Electronics* 38(1):15–20.

Arai, H., Tanie, K., and Tachi, S. 1993. Dynamic control of a manipulator with passive joints in operational space. *IEEE Transactions on Robotics and Automation* 9(1):85–93.

Bergerman, M., and Xu, Y. 1996. Robust joint and Cartesian control of underactuated manipulators. *ASME Journal of Dynamic Systems, Measurement, and Control* 118:557–565.

Bergerman, M., and Xu, Y. 1998. Optimal control of manipulators with any number of passive joints. *Journal of Robotic Systems* 15(3):115–129.

English, J. D., and Maciejewski, A. A. 1997. Robotic workspaces after a free-swinging failure. *Journal of Intelligent and Robotic Systems* 19(1):55–72.

English, J. D., and Maciejewski, A. A. 1998. Fault tolerance for kinematically redundant manipulators: Anticipating free-swinging joint failures. *IEEE Transactions on Robotics and Automation* 14:566–575.

English, J. D., and Maciejewski, A. A. 2000a. Measuring and reducing the Euclidean-space measures of robotic joint

failures. *IEEE Transactions on Robotics and Automation* 16(1):20–28.

English, J. D., and Maciejewski, A. A. 2000b. On the implementation of velocity control for redundant manipulators. *IEEE Transactions on Systems, Man, and Cybernetics—Part A: Systems and Humans* 30:233–237.

Lewis, C. L., and Maciejewski, A. A. 1994. Dexterity optimization of kinematically redundant manipulators in the presence of failures. *Computers and Electrical Engineering* 20:273–288.

Lewis, C. L., and Maciejewski, A. A. 1997. Fault tolerant operation of kinematically redundant manipulators for locked joint failures. *IEEE Transactions on Robotics and Automation* 13:622–629.

Liégeois, A. 1977. Automatic supervisory control of the configuration and behavior of multibody mechanisms. *IEEE Transactions on Systems, Man, and Cybernetics* SMC-7:868–871.

Maciejewski, A. A. 1991. The design and control of fault tolerant robots for use in hazardous or remote environments. *Proceedings of the Fourth American Nuclear Society Topical Meeting on Robotics and Remote Systems*, Albuquerque, NM, February 24-28, pp. 633–642.

Morecki, A., and Knapczyk, J. 1999. *Basics of Robotics.* New York: Springer-Verlag.

Oriolo, G., and Nakamura, Y. 1991. Control of mechanical systems with second-order nonholonomic constraints: Underactuated manipulators. *Proceedings of the 30th Conference on Decision and Control*, Brighton, UK, December 11-13, pp. 2398–2403.

Paredis, C.J.J., Au, W.K.F., and Khosla, P. K. 1994. Kinematic design of fault tolerant manipulators. *Computers and Electrical Engineering* 20:211–220.

Paredis, C.J.J., and Khosla, P. K. 1994. Mapping tasks into fault tolerant manipulators. *Proceedings of the IEEE International Conference on Robotics and Automation*, San Diego, CA, May 8-13, pp. 696–703.

Paul, R. P. 1981. *Robot Manipulators: Mathematics, Programming, and Control.* Cambridge, MA: MIT Press.

Roberts, R. G. 1996. On the local fault tolerance of a kinematically redundant manipulator. *Journal of Robotics Systems* 13:649–661.